Nanoscale heterogeneities in CeO_2–ZrO_2 nanocrystals highlighted by UV-resonant Raman spectroscopy†

Takaaki Taniguchi,[a] Tomoaki Watanebe,[b] Satoshi Ichinohe,[b] Masahiro Yoshimura,[a] Ken-ichi Katsumata,[a] Kiyoshi Okada[a] and Nobuhiro Matsushita*[a]

Received 20th January 2010, Accepted 6th April 2010
DOI: 10.1039/c0nr00040j

Selection of the excitation wavelength at nonresonant and resonant Raman conditions provided detection selectivity in the tetragonal and cubic phases in CeO_2–ZrO_2 nanocrystals, respectively. It was suggested that cubic-phase domains containing Ce^{3+} deficiencies were involved in the tetragonal-phase matrix.

Recently, much effort has been expended to decrease the emission of pollutant gases such as CO, NO_x, and hydrocarbons for the protection of the global environment. CeO_2-based materials offer properties suitable for a three-way catalyst for treating exhaust gasses from automobiles, owing to their oxygen storage capacities (OSC) and redox properties from the reversible oxidation/reduction of $Ce^{4+} \leftrightarrow Ce^{3+}$.[1] In particular, researchers have intensively investigated CeO_2–ZrO_2 mixed oxides due to their efficient catalytic properties.[2]

Several contributions of Zr^{4+} substitution have been suggested for the enhancement of catalytic properties. For example, such substitutions can strongly suppress the sintering of the catalyst and loss of performance over time at elevated temperatures, so maintaining the surface area (or number of active surface sites) of the initial materials.[2] These substitutions also impact the crystalline phase; the materials crystallize into monoclinic and cubic as well as tetragonal phases involving metastable t' and t'' phases,[3] depending on the chemical composition and the preparative method. These diverse structural alternatives also relate to the enhancement of the catalytic properties.

In addition to these traditional mechanisms, Mamontv *et al.* recently suggested that $Ce_{0.5}Zr_{0.5}O_2$ nanocrystals exhibit two crystalline and/or compositional phases in an identical grain, and such nanoscale heterogeneities play a key role in the enhancement of the performance on the basis of a pair-distribution function (PDF) analysis using neutron-diffraction data and a temperature programmed reduction (TPR) analysis.[4] Montini *et al.* further supported this structural model by using site-selective Eu^{3+} luminescence.[5] However, the heterogeneities were so complex that neither Mamontv's nor Montini's work yielded any identification of a secondary phase, whereas the primary t'' phase must have been contained. Furthermore, neither suggested a formation mechanism.

In this communication, we investigated the debatable aspects of these materials by using UV-Raman spectroscopy with a 363.8 nm laser line. Raman spectroscopy is an available, nondestructive, and rapid analytical technique for investigating the electronic and phonon structures of materials. These excellent characteristics have motivated intensive Raman studies for CeO_2-based materials.[6] Moreover, we recently demonstrated that when the band-gap energy of pure and Re^{3+} doped CeO_2 materials matched the UV-excitation energy (363.8 nm in wavelength), the second order Raman bands were dramatically enhanced.[7] Owing to the resonant Raman effect, we succeeded in the identification of the local-defect structure in the materials. Herein, we employed this effective analytical method for the investigation of the structural properties of CeO_2–ZrO_2 nanocrystals and discussed the nanoscale heterogeneities involved.

We prepared $Ce_{1-x}Zr_xO_2$ nanocrystals in which $x = 0$, 0.5, or 0.8, using a hydrothermal method at 200 °C for 6 h and subsequent annealing at 800 °C for 5 h. (The experimental details are provided in the ESI†.) According to the phase diagram, CeO_2 in a cubic phase was thermodynamically stable at room temperature, while $Ce_{0.5}Zr_{0.5}O_2$ and $Ce_{0.2}Zr_{0.8}O_2$ were metastable. Among these compounds, $Ce_{0.5}Zr_{0.5}O_2$ is most important for catalysis as it is expected to offer the most useful properties in a binary system.

First, we employed conventional analytical methods (X-Ray Diffraction (XRD) and visible-Raman spectroscopy) to evaluate the overall structural properties; this approach was first developed by our

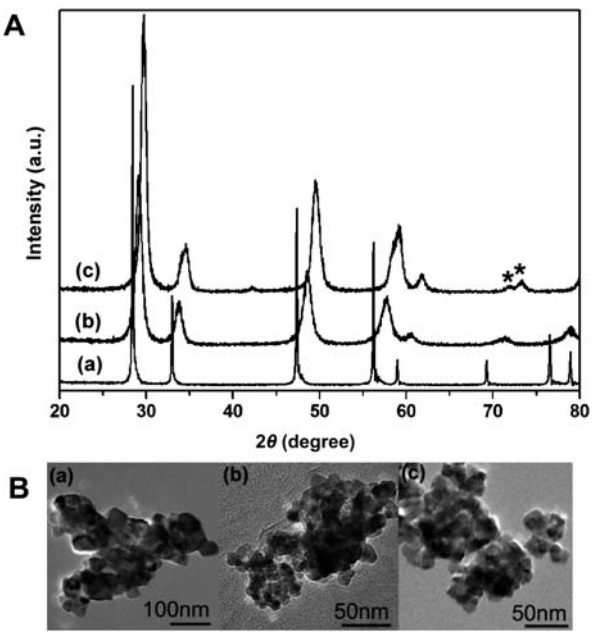

Fig. 1 (A) XRD patterns and (B) TEM images of (a) CeO_2, (b) $Ce_{0.5}Zr_{0.5}O_2$ and (c) $Ce_{0.2}Zr_{0.8}O_2$nanocrystals. Asterisks present (004)/(400) tetragonal (t') distortion.

[a]*Materials and Structures Laboratory, Tokyo Institute of Technology, 4259 Nagatsuta, Midori-ku, Yokohama, 226-8503, Japan*
[b]*Department of Applied Chemistry, School of Science and Technology, Meiji University, 1-1-1 Higashimita, Tama-ku, Kawasaki, 214-8571, Japan*
† Electronic supplementary information (ESI) available: Preparation procedures and measurement conditions. See DOI: 10.1039/c0nr00040j

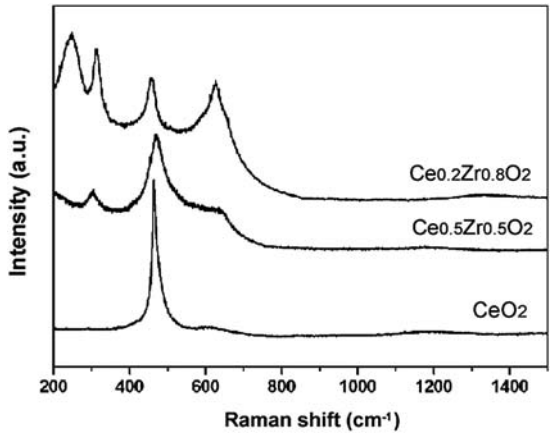

Fig. 2 Vis Raman spectra of CeO_2–ZrO_2 nanocrystals.

group[3] and has become very common for the phase analysis of CeO_2–ZrO_2 materials. Fig. 1A shows XRD patterns of the CeO_2–ZrO_2 nanocrystals. The crystallite sizes were 59.8, 10.3, and 13.2 nm for the CeO_2, $Ce_{0.5}Zr_{0.5}O_2$, and $Ce_{0.2}Zr_{0.8}O_2$ samples, respectively, using the Debye–Scherrer formula. These sizes generally correspond well to those observed by transmission electron microscopy (see Fig. 1B). The patterns of $Ce_{1-x}Zr_xO_2$ ($x = 0$ or 0.5) and $Ce_{0.2}Zr_{0.8}O_2$ corresponded to the cubic and tetragonal (t') phases, respectively, while visible-Raman spectra (Fig. 2) indicated that cubic and tetragonal phases are formed for pure CeO_2 and the other samples, respectively.[3] A summary of these results indicated that CeO_2, $Ce_{0.5}Zr_{0.5}O_2$, and $Ce_{0.2}Zr_{0.8}O_2$ exhibit cubic, t'', and t' phases, respectively. These results were in good agreement with the previous studies,[8] and the nanoscale heterogeneities were not detectable by the conventional analytical methods.

We investigated the optical absorption properties by UV-Vis diffuse reflection spectroscopy. As shown in Fig. 3, the Zr^{4+} substitution yielded no significant alterations in the optical absorption properties so that the excitation energy was comparable with the band-gap energy, ensuring that the UV-excitation energy was well matched to the resonant Raman conditions of all the samples.

Fig. 4 displays the UV-Raman spectra. Owing to the resonant Raman effects, the features shown in these spectra were different from those seen in the visible spectra. The first notable point was that

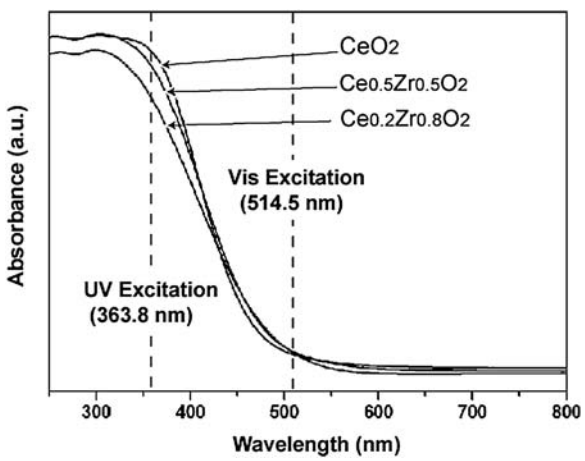

Fig. 3 UV-Vis diffuse reflection spectra of CeO_2–ZrO_2 nanocrystals.

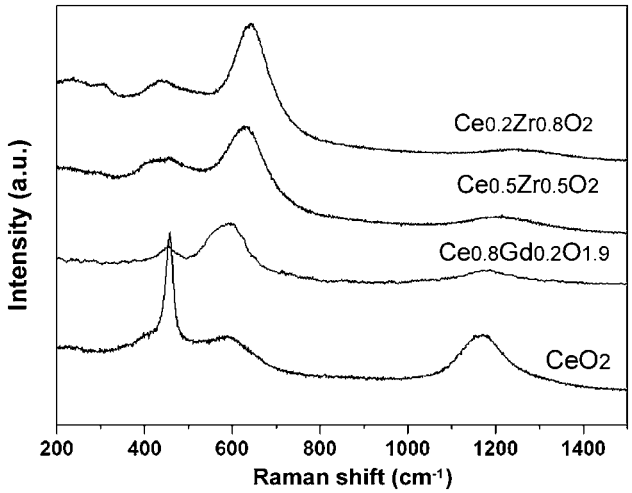

Fig. 4 UV Raman spectra of CeO_2–ZrO_2 nanocrystals. Note that UV Raman spectra of 3.2 nm $Ce_{0.8}Gd_{0.2}O_{1.9}$ nanocrystals are shown for comparison.

we observed the low frequency bands (approximately 250 and 302 cm^{-1}) from the tetragonal phase only in the $Ce_{0.2}Zr_{0.8}O_2$ sample, while the peaks at approximately 600 cm^{-1} and 1200 nm^{-1} appeared for all samples. The bands at 600 cm^{-1} and 1200 nm^{-1} corresponded to the defect-induced (D) band and second overtone band of the longitudinal optic (2LO) mode in the cubic phase, respectively, which would be strongly enhanced in the resonant Raman condition.[7] In fact, the $Ce_{0.5}Zr_{0.5}O_2$ nanocrystals show similar spectra to UV spectra of $Ce_{0.8}Gd_{0.2}O_{1.9}$ nanocrystals with the cubic phase studied in our earlier work.[7] Therefore, the presence of these bands indicated that the $Ce_{0.5}Zr_{0.5}O_2$ nanocrystals, previously assigned as the t'' phase, involve a secondary phase identified as a cubic phase. We highlight this heterogeneity for the first time in the present study. Furthermore, the strong detection of bands from the cubic phase, even in Zr-rich t' phase samples ($Ce_{0.2}Zr_{0.8}O_2$), demonstrated that UV-Raman spectroscopy can selectively detect a cubic phase, while visible spectroscopy is sensitive to the tetragonal phase.

Careful investigation of the spectra revealed a detailed structure of the cubic phase. As shown in the UV-Raman spectra, the Raman active F_{2g} band at 470 cm^{-1} from the cubic phase broadened and weakened, while the defect-related bands at 400 cm^{-1} and 600 cm^{-1} grew more pronounced with increasing Zr^{4+} concentration. These trends indicated that Zr^{4+} doping induced defects in the cubic structure. Particularly, the band at 600 cm^{-1} was due to the Ce^{3+} deficiency,[6,7] indicating a Zr^{4+} substitution induced Ce^{3+} deficiency in the cubic domain. Note that the pure ceria nanoparticles also show the band in the resonant Raman spectra because of the presence of Ce^{3+} spices due to the size effect.[7] However, the relative band intensity of the band to the F_{2g} band observed in the $Ce_{0.5}Z_{0.5}O_2$ sample is much higher than smaller undoped-ceria nanoparticles (*ca.* 5 nm size),[7] which indicates that the size effect or high surface area is not the predominant reason for the strong detection of the Ce^{3+}-related band in the resonant Raman spectra of CeO_2–ZrO_2 solid solution nanocrystals. Based on the X-ray absorption fine structure (XAFS) analysis, Zhang *et al.* have also observed the increase in the Ce^{3+} concentration with Zr^{4+} doping.[9] They have suggested that Ce^{3+} (1.039 Å) with a larger ionic radius than both Ce^{4+} (0.97 Å) and Zr^{4+} (0.84 Å) was formed to decrease the total lattice-strain energy that

accumulated due to the large interval between the ionic radii of Ce^{4+} and Zr^{4+}.

Along with the band intensity at 600 cm^{-1}, the band position showed a strong dependency on the chemical composition. The bands clearly shifted toward a higher energy level with an increase in the Zr^{4+} concentration. For the CeO_2–ZrO_2 binary system, the lattice shrinkage occurred due to the substitution of the larger Ce^{4+} ion by the smaller Zr^{4+} ion as clearly shown in the higher-angle shift of the diffraction peak with an increasing Zr^{4+} concentration (Fig. 1). This substitution would result in the reduced average length of the M–O bond (M = Ce or Zr). Consequently, the force constants corresponding to the vibrations of the M–O bond would increase, leading to the detectable high-energy shift in the Raman band. Note that we observed the same tendency in the band position for the 2LO band (1200 cm^{-1}), which also indicated an increase of the phonon energy in the cubic phase with Zr^{4+} substitution. On this basis, the high-energy shift in the Raman band positions with Zr^{4+} substitution, accompanying the lattice shrinkage, supported the possibility that the phase heterogeneities were involved in an identical grain rather than being present in separate grains. Summarizing the current and previous studies available so far, we suggest that the cubic-phase nanodomains involving Ce^{3+} cations formed within the tetragonal-phase matrix, and as a result, the lattice strain in the mixed oxides was relaxed. This mechanism has a possibility for the formation of heterogeneities in CeO_2–ZrO_2 nanocrystals, presumably contributing to their efficient redox properties.

In conclusion, we employed UV-resonance Raman spectroscopy to come to an in-depth understanding of the local structure of the $Ce_{1-x}Zr_xO_2$ nanocrystalline catalysis. For the first time, this novel, simple, and effective method clarified the presence of a secondary phase identified as the cubic phase in mixed oxide nanocrystals even in cases where they are characterized as the t' or t'' phase by XRD and visible-Raman spectroscopy. Furthermore, we revealed that the cubic phase contained Ce^{3+} cations, which likely relaxed the lattice strain accumulated due to the large interval between the Ce^{4+} and the Zr^{4+} ions in ionic radii. The high-energy shift in the Raman band positions with Zr^{4+} substitution indicated that the cubic and tetragonal phases coexisted in an identical grain. Owing to the availability and excellent detection sensitivity of the local structure, combination analysis using visible- and UV-Raman spectroscopy was very useful in studying the structural properties of $Ce_{1-x}Zr_xO_2$ catalysis at the nanoscale.

Notes and references

1 (*a*) J. Kaspar, P. Fornasiero and M. Graziani, *Catal. Today*, 1999, **50**, 285; (*b*) A. Trovarelli, C. de Leitenburg, M. Boaro and G. Dolcetti, *Catal. Today*, 1999, **50**, 353.
2 R. Di Mont and J. Kaspar, *J. Mater. Chem.*, 2005, **15**, 633.
3 M. Yashima, H. Arashi, M. Kakihana and M. Yoshimura, *J. Am. Ceram. Soc.*, 1994, **77**, 1067.
4 E. Mamontov, R. Brezny, M. Koranne and T. Egami, *J. Phys. Chem. B*, 2003, **107**, 13007.
5 T. Montini, A. Speghini, L. De Rogatis, B. Lorenzut, M. Bettinelli, M. Graziani and P. Fornasiero, *J. Am. Chem. Soc.*, 2009, **131**, 13155.
6 (*a*) J. E. Spanier, R. D. Robinson, F. Zheng, S. W. Chan and I. P. Herman, *Phys. Rev. B: Condens. Matter*, 2001, **64**, 245407; (*b*) A. Nakajima, A. Yoshihara and M. Ishigame, *Phys. Rev. B: Condens. Matter*, 1994, **50**, 13297; (*c*) W. H. Weber, K. C. Hass and J. R. McBride, *Phys. Rev. B: Condens. Matter*, 1993, **48**, 178.
7 T. Taniguchi, T. Watanabe, N. Sugiyama, A. K. Subramani, H. Wagata, N. Matsushita and M. Yoshimura, *J. Phys. Chem. C*, 2009, **113**, 19789.
8 (*a*) A. Ahniyaz, T. Watanabe and M. Yoshimura, *J. Phys. Chem. B*, 2005, **109**, 6136; (*b*) F. Zhang, C. H. Chen, J. C. Hanson, R. D. Robinson, I. P. Herman and S. W. Chan, *J. Am. Ceram. Soc.*, 2006, **89**, 1028.
9 F. Zhang, C. H. Chen, J. M. Raitano, J. C. Hanson, W. A. Caliebe, S. Khalid and S. W. Chan, *J. Appl. Phys.*, 2006, **99**, 084313.

